Inorganic Chemistry

Article

pubs.acs.org/IC

Synthesis, Crystal Structure, and Photoluminescence Studies of a Ruthenocenyl-Decorated Sn/S Cluster

Eliza Leusmann,[†] Mona Wagner,[†] Nils W. Rosemann,[‡] Sangam Chatterjee,[‡] and Stefanie Dehnen*[,†]

[†]Fachbereich Chemie and Wissenschaftliches Zentrum für Materialwissenschaften, Philipps-Universität Marburg, Hans-Meerwein-Str., D-35043 Marburg, Germany

[‡]Fachbereich Physik und Wissenschaftliches Zentrum fuï Materialwissenschaften, Philipps-Universität Marburg, Renthof 5, D-35032 Marburg, Germany

Supporting Information

ABSTRACT: Recently, we reported on ferrocenyl-decorated Sn/S clusters; herein, we present the extension of our investigations by attachment of ruthenocenyl units to an according cluster skeleton. The latter was realized upon improvement of the synthesis of acetylruthenocene, its conversion to a hydrazone derivative, and the subsequent reaction with a keto-functionalized Sn/S precursor complex. The report comprises the crystal structures of acetylruthenocene and the ruthenocenyl-terminated Sn/S cluster $[(R^{Rc}Sn)_4Sn_2S_{10}]$ (R^{Rc} = $CMe_2CH_2C(Me)$=N−N=C(Me)-Rc), as well as the discussion of the electrochemical properties of the latter and its behavior during time-resolved photoluminescence investigations.

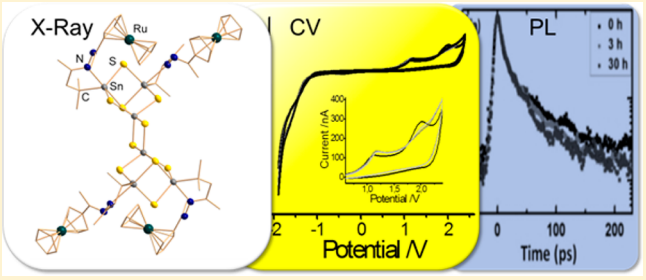

INTRODUCTION

Since the discovery of ferrocene in 1951,[1] metallocenes have been molecules of great interest. Their high stability, in the case of ferrocene even to air and moisture, turns them into useful complexes for diverse studies. The relatively simple synthesis provides the opportunity to introduce different central metal ions, thereby generating metallocene complexes with different chemical and physical properties. For instance, derivatizations of ruthenocene, which was first synthesized in 1952,[2] require completely different reaction conditions.[3] Today, ferrocene has a long tradition as a functional ligand to inorganic nanoclusters, boranes, fullerenes, porphyrines, or other (bio)organic molecules,[4,5] whereas the attachment of ruthenocene units has remained much rarer. Besides combinations with fullerenes or (bio)organic devices,[6] some examples are known that represent attachments to metal atoms or functionalization of nanoclusters.[7]

Thiometallates, including thiostannates, were comprehensively investigated by Krebs et al.,[8] who reported the synthesis and structures of anions like $[Sn_4S_{10}]^{4-}$ with adamantane-like structures. Berwe and Haas showed some years later that organotin trihalides, with ligands R such as C_6H_5, 2,4,6-$(Me)_3C_6H_2$, $C_{10}H_7$, CF_3, C_6F_5, and $C(SiMe_3)_3$, readily react with sulfide sources to produce uncharged complexes of the type $[(RSn)_4S_6]$, the inorganic core of which adopts adamantane-type topology.[9a] Along with further contributions to this class of compounds,[9b−d] these studies confirmed earlier work that suggested an according cluster topology without crystallographic proof.[9e,f]

During the past years, several complexes were presented being decorated by functional organic ligands R^f, most of which prefer a double-decker-like complex structure due to an intramolecular back-coordination of the donor atoms in R^f to the Sn atoms of the Sn/S core.[10] The functional groups, such as keto groups or hydrazine groups in $[(R^1Sn)_4S_6]$ with R^1 = CMe_2CH_2COMe (**A**) or $CMe_2CH_2C(Me)NNH_2$ (**B**) enable further derivatization.[10,11]

Our interest in the connection of metal complexes to Sn/S cages via organic ligands aims toward the generation of core−shell−shell molecules, which consist of an inorganic core, an interjacent organic shell, and a metal complex termination for studying any electronic communication between the chalcogenide core, which refers to the semiconductor material SnS_2,[12] and the metal atoms on the surface—with or without illumination or additional electrochemical treatment. We have recently reported the first examples of ferrocenyl-decorated Sn/S complexes with monofunctionalized ferrocenyl ligands as in $[(R^{Fc}Sn)_4Sn_2S_{10}]$ (R^{Fc} = $CMe_2CH_2C(Me)$=N−N=C(Me)-Fc) or bis-functionalized ones as in $[(R^{fC1}Sn_2)_2S_4]$ or $[(R^{fC2}Sn_2)_2S_4]$ (R^{fC1} = $[CMe_2CH_2C(Me)$=N−N=C(H)$]_2$fC; R^{fC2} = $[CMe_2CH_2C(Me)$=N−NHC(O)$]_2$fC).[13] These studies extended Fc-Sn chemistry in general[14] and previous work on the influence of the organic moiety on the structure of Sn/S complexes in particular. Herein, we present the first attachment of ruthenocene units to an Sn/S cluster core in the novel complex $[(R^{Rc}Sn)_4Sn_2S_{10}]$ (R^{Rc} = $CMe_2CH_2C(Me)$=N−N=

Received: February 14, 2014
Published: April 9, 2014

   dx.doi.org/10.1021/ic500367y | Inorg. Chem. 2014, 53, 4228−4233

Table 1. Crystallographic and Refinement Details of 1 and 2.

	compound **1**	compound **2**
chemical formula	$C_{12}H_{12}O_1Ru_1$	$C_{72}H_{92}N_8Ru_4S_{10}Sn_6$
formula mass (g mol^{-1})	273.29	2506.55
crystal color and shape	colorless block	colorless plate
crystal size (mm^3)	0.24 × 0.08 × 0.07	0.27 × 0.13 × 0.05
crystal system	monoclinic	triclinic
a, b, c (Å)	12.584(3), 13.521(3), 5.7647(12)	11.3247(8), 11.4359(8), 21.0917(15)
α, β, γ (deg)	90, 90.27(3), 90	95.154(6), 102.536(5), 92.727(6)
V (Å^3)	980.8(4)	2649.3(3)
space group, Z	$P2_1/c$, 4	$P\bar{1}$, 1
abs. coefficient μ (mm^{-1})	1.557	2.173
abs. correction type	none	numerical
T_{min}, T_{max}		0.5932, 0.8005
θ range (deg)	2.21−26.77	1.79−26.71
reflections measured	7188	11 191
independent reflections	2070	11 171
R_{int}	0.0656	0.0990
R_1 ($I > 2\sigma(I)$)/$wR(F^2)$ (all data)	0.0230/0.0508	0.0472/0.1357
goodness of fit on F^2	0.836	0.895
largest diff. peak/hole (e$^-$ Å^{-3})	0.49/−0.64	1.08/−1.63

C(Me)Rc), as a proof of principle, and furthermore demonstrate its consequences regarding the cluster stability under different conditions including electrochemical treatment and laser irradiation—also in comparison with the ferrocenyl-decorated analogue.

EXPERIMENTAL SECTION

General. All reaction steps were carried out under Ar atmosphere. All solvents were dried and freshly distilled prior to use. The precursor $[(R^1Sn)_4S_6]$ (**A**; R^1 = $CMe_2CH_2C(Me)O$) was prepared according to the reported methods.[10b] Ruthenocene was prepared by the method given by Vol'kenau et al.,[3b] apart from the use of toluene instead of benzene. The yellow crystalline powder was analyzed by mass spectrometry. Electron ionization (EI) ($C_{10}H_{10}Ru$): calculated m/z 231.9826, measured m/z 231.9828.

Synthesis of {(C_5H_5)Ru[$C_5H_4C(O)Me$]} (Rc^{Ac}, 1). Acetylruthenocene (**1**) was synthesized according to a modified version of the protocol published by Rausch et al.:[3a] Ruthenocene (1 equiv, 1 g, 4.31 mmol) was dissolved in 40 mL of absolute CH_2Cl_2. Freshly distilled acetylchloride (1.5 equiv, 0.51 g, 6.47 mmol) was added, and the solution was cooled to −78 °C. Subsequently, $AlCl_3$ (2.05 equiv, 1.18 g, 8.84 mmol) were added. The solution initially became cloudy, but cleared up to turn bright yellow within five minutes. This solution was stirred for further 5 min and was then poured into 75 mL of ice water. The mixture was extracted with 80 mL of CH_2Cl_2 for three times, dried over Na_2SO_4, and concentrated *in vacuo*. The solid was purified by silica column chromatography (ethanol). By concentration *in vacuo* compound **1** was obtained as a yellow powder in 80% yield (3.45 mmol, 593 mg). Electrospray ionization (ESI)$^+$($C_{12}H_{12}Ru_1O_1Na$): found: m/z 296.9821 (100% relative abundance), calculated 296.9827. For single-crystalline material, the powder was redissolved in ethanol, which was slowly evaporated thereupon. ESI$^+$ mass spectrum of compound **1** in CH_2Cl_2, $C_{12}H_{12}O_1Ru_1Na_1$: calculated m/z 296.9827, measured m/z 276.9821.

Synthesis of [(RcC(Me)═N−N═CMeCH$_2$CMe$_2$Sn)$_4$Sn$_2$S$_{10}$] (2). Acetylruthenocene (compound **1**; 1 equiv, 60 mg, 0.22 mmol) was dissolved in 5 mL of absolute ethanol and CH_2Cl_2 (1:1). To the yellowish solution, 5 mL of N_2H_4 in tetrahydrofuran (THF) (1 M) was added, and the solution was stirred for 8 h. The solvent was removed *in vacuo*, and the remaining residue was dried for 3 h under reduced pressure (1 × 10^{-3} mbar). Subsequently, **A** (0.25 equiv, 58.4 mg, 0.055 mmol) was added as solid to the hydrazone-functionalized acetylruthenocene derivative. After concentration of the mixture for 30 min at 1 × 10^{-3} mbar, 10 mL of CH_2Cl_2 was added, and the solution was allowed to stir for 12 h in the dark; under daylight, the precipitation of tin sulfide indicates decomposition of the reaction mixture and/or the product. Traces of tin sulfide were then filtered off under exclusion of light, and the filtrate was layered with 20 mL of toluene. After three months in the dark, yellow crystals of **2** were obtained in approximately 37% yield besides a newly formed precipitate of SnS_2. The composition of the title compound was confirmed by means of energy dispersive X-ray (EDX) spectroscopy. ESI$^+$ mass spectrum of $[C_{54}H_{70}N_6Ru_3S_4Sn_3]^+$: calculated m/z 1590.8772, measured m/z 1590.8723; further fragments: $[C_{42}H_{59}N_6Ru_2S_4Sn_3]^+$: calculated m/z 1334.8855, measured m/z 1334.8854, $[C_{30}H_{49}N_6RuS_4Sn_3]^+$: calculated m/z 1078.9016, measured m/z 1078.9023.

Spectroscopy and Spectrometry. ^{1}H NMR, ^{13}C NMR, and ^{119}Sn NMR measurements were carried out using a Bruker DRX 300 and 400 MHz spectrometer at 25 °C. In ^{1}H and ^{13}C NMR spectra, chemical shifts were quoted in ppm relative to the residual protons of deuterated solvents. For ^{119}Sn NMR measurements, Me_4Sn was used as internal standard.

Mass spectrometry (MS) was performed on a Finnigan MAT 95S. Electrospray ionization mass spectrometry (ESI-MS) was performed on a Finnigan LTQ-FT spectrometer by Thermo Fischer Scientific in the positive ion mode with solvent as carrier gas.

X-ray Diffraction Measurement, Structure Solution, and Refinement Details. Data were collected on a diffractometer equipped with an STOE imaging plate detector system IPDS2T, using Mo Kα radiation with graphite monochromatization (λ = 0.710 73 Å) at 100 K. The structure solution was performed using direct methods, full-matrix-least-squares refinement against F^2, using SHELXTL software and the OLEX2 software package.[15,16] Details of the data collections and refinements are given in Table 1.

All atoms within the crystal structure of compound **1** were refined by using anisotropic displacement parameters. The packing of the acetylruthenocene molecules in the crystal structure of compound **1** allows for an optimization of the intermolecular interactions via hydrogen bridges (Supporting Information, Figure S1). All atoms within the crystal structure of compound **2** were refined by using anisotropic displacement parameters, except the atoms of solvent molecules that could not be localized due to heavy disorder. The electron density of these atoms was therefore omitted during the refinement procedure using the SQUEEZE routine.

dx.doi.org/10.1021/ic500367y | Inorg. Chem. 2014, 53, 4228−4233

RESULTS AND DISCUSSION

To modify the metal complex attached to the core−shell substructure, we intended to introduce ruthenocene (Rc) units, which are much more rarely found as terminal ligands to inorganic clusters or complexes.[7] To provide a group of complementary functionality we generated acetylruthenocene $\{(C_5H_5)Ru\text{-}[C_5H_4C(O)Me]\}$ (Rc^{Ac}, **1**) in a first step, as a precursor to the corresponding hydrazone, which was assumed to be reactive toward **A**. For that, we followed a synthesis protocol for acetylruthenocene reported by Rausch et al.,[3a] which was, however, modified to shorten the reaction time. Instead of acetanhydride, we used acetylchloride, which was reacted with ruthenocene and $AlCl_3$ in dichloromethane for 15 min at −78 °C. After quenching the solution with ice water and using column chromatography for purifying, compound **1** was obtained in 80% yield (Scheme 1).

Scheme 1. Reaction Scheme for the Synthesis of Acetylruthenocene (1)

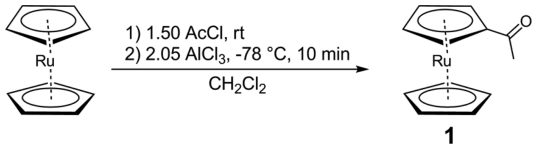

In addition, it was possible to grow single crystals of **1** and thus to provide the previously unknown single-crystal structure of acetylruthenocene. Compound **1** (Figure 1) crystallizes in

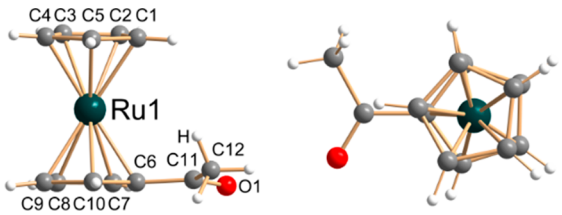

Figure 1. Molecular structure of acetylruthenocene (**1**) in two different views.

the monoclinic space group $P2_1/c$ with four molecules within the unit cell (a = 12.584(3) Å, b = 13.521(3) Å, c = 5.7647(12) Å, β = 90.27(3)°, V = 980.8(4) Å^3). The distances between the cyclopentadienyl (Cp) ring centroids and the Ru atom range between 1.8158(4) Å for $[C_5H_4C(O)Me]$-Ru and 1.8164(4) Å for (C_5H_5)-Ru (c.f. distances in $(C_5H_5)_2Ru$ 1.8412(3)/1.8442(3) Å[17]). In contrast to $(C_5H_5)_2Ru$, the two Cp rings in **1** are not exactly coplanar but are somewhat tilted toward each other, including an angle of 3.87° as a result of the nonsymmetric substitution pattern. In addition, while the Cp rings in $(C_5H_5)_2Ru$ possess a nearly perfect ecliptic orientation (twist angle 1.23°), the Cp rings in **1** are staggered by about 4.83−5.73°. The acetyl group is tilted a little bit out of the plane spanned by the adjacent Cp ring in that the C6−C11 bond is rotated by 6.48°.

Reaction of **1** with hydrazine N_2H_4 in THF led to the formation of the corresponding hydrazone $\{(C_5H_5)Ru[C_5H_4\text{-}C(Me)NNH_2]\}$ (Rc^{AcNNH2}, **1′**), which reacts with **A** *in situ*. Under rearrangement of the inorganic cluster core into a $[Sn_6S_{10}]$ architecture that represents two doubly (μ-S)-bridged defect heterocubanes, four of the hydrazone-derivatized acetylruthenocene molecules were attached to the Sn/S cage via condensation to form the air-sensitive compound $[(R^{Rc}Sn)_4Sn_2S_{10}]$ (**2**; R^{Rc} = $CMe_2CH_2C(Me)$=N−N=C(Me)Rc; Scheme 2). The compound crystallizes with one formula unit in the unit cell in the triclinic space group $P\bar{1}$ (a = 11.3247(8) Å, b = 11.4359(8) Å, c = 21.0917(15) Å, V = 2649.3(3) Å^3). Figure 2 shows the molecular structure of **2**.

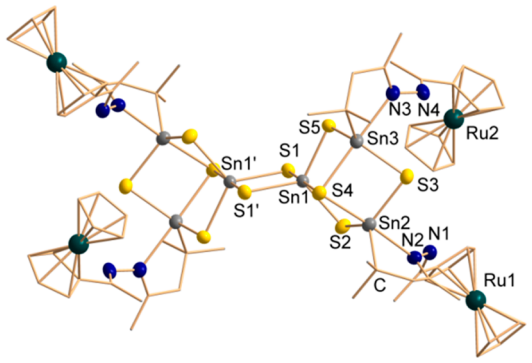

Figure 2. Molecular structure of $[(RuAcN{=}NCMeCH_2CMe_2)_2Sn_3S_4(\mu\text{-}S)]_2$ (**2**). H atoms are omitted for clarity.

The rearrangement $[Sn_4S_6] \rightarrow [Sn_6S_{10}]$ occurred due to the size and rigidity of the metallocene molecules,[9a,f,10,13] similar to the situation observed recently for corresponding ferrocenyl-decorated systems. Each Sn atom is five-coordinated in a distorted trigonal-bipyramidal manner, either by three sulfide ligands, one carbanion ligand C atom, and one of the azine N atoms (Sn2, Sn3), or by five sulfide ligands (Sn1). Sn−S bond lengths vary between 2.402(2) Å (Sn2−S2) and 2.8246(2) Å (Sn1−S4). The complex is not particularly stable, as it is split into defect-heterocubane fragments $[(Ru^{Ac}N{=}NCMe\text{-}$

Scheme 2. Nonstoichiometric Reaction Scheme for the Synthesis of $[(R^{Rc}Sn)_4Sn_2S_{10}]$ (2)[a]

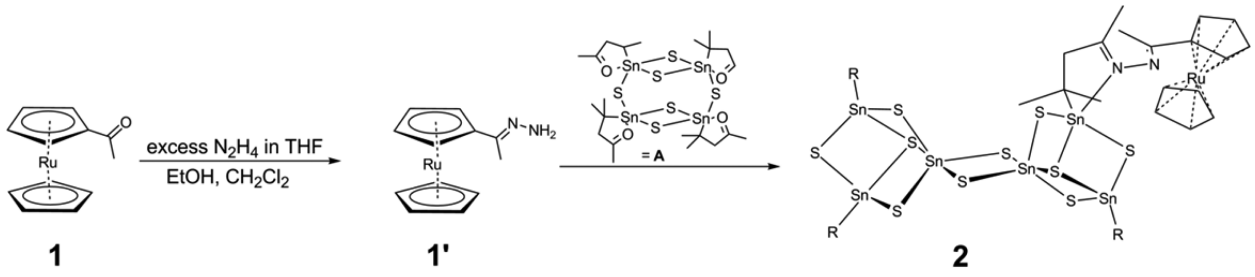

[a] R^{Rc} = $CMe_2CH_2C(Me)$=N−N=C(Me)Rc); the ruthenocenyl-terminated organic group is shown explicitly for one of the four ligands. Both steps occur under release of water; the second step additionally affords tin(II)sulfide, mesityloxide, and hydrogen as further byproducts.

dx.doi.org/10.1021/ic500367y | Inorg. Chem. 2014, 53, 4228−4233

$CH_2CMe_2Sn)_3S_4]^+$ (**2′**) under ESI-MS conditions in CH_2Cl_2 (m/z measured 1590.8723 at 19% relative abundance, calculated 1590.8772); a mass peak of compound **2** was not observed. Further dominant peaks at m/z 1334.8854 and 1078.9023 can be assigned to heterocubane-type fragments like **2′**, however, upon loss of one or two ruthenocene moieties. It cannot be excluded that **2** and **2′** coexist in solution. The ^{119}Sn NMR spectrum of a CD_2Cl_2 solution of single crystals of **2** exhibits two signals, at −96 ppm and −113 ppm, and a hint toward a further signal around −98.5 ppm. This may indicate the presence of **2** (with two distinct Sn sites) or a mixture of **2** and **2′** (with the chemical shifts of the Sn atoms in the SnS_3CN environment being similar in both complexes). However, on the basis of the poor quality of the ^{119}Sn spectrum, the assignment of the peaks needs to be viewed as a suggestion rather than as a clear proof. Rough estimation of the intensities of the peaks indicate the latter.

To judge the electrochemical stability of the compound, also on comparison with the analogous ferrocenyl-decorated complex,[13b] we carried out cyclic voltammetry (CV) experiments of a solution of **2** in CH_2Cl_2 with $[NBu_4][PF_6]$ as electrolyte. Only a qualitative picture can be drawn from these measurements, since the sample decomposes at the addition of ferrocene as internal reference (see Supporting Information, Figure S9); therefore, Figure 3 shows the voltammogram

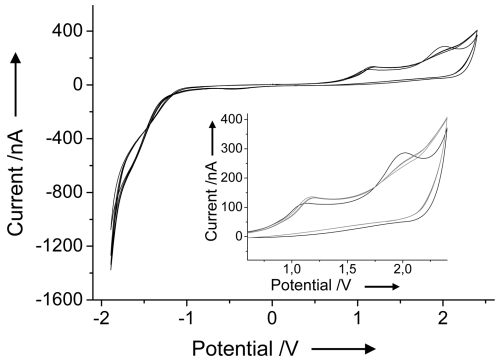

Figure 3. Cyclic voltammogram recorded at a platinum electrode on a CH_2Cl_2 solution of **2** (5 mM) in the presence of $[NBu_4][PF_6]$ (50 mM) without internal reference. (inset) The oxidation peak, with the first cycle shown in black. Scan range and rate: −1.89 to 2.4 V, 0.05 V s^{-1}.

without ferrocene. One observes two irreversible oxidation peaks at 1.13 V (113.8 nA) and 2.02 V (286.2 nA) during the first cycle. After the first cycle, the first oxidation peak is shifted to 1.18 V (135.9 nA), and the second oxidation diminishes to become a shoulder, which points toward decomposition—maybe under formation of dimeric moieties, such as those known for isolated ruthenocene.[18]

The corresponding ferrocenyl-decorated Sn/S complex, in contrast, showed a well-cyclable behavior and a lower oxidation potential. Both features are in agreement with the differences between ferrocene and ruthenocene alone: oxidation of the latter is known to produce a ruthenocenium ion that readily undergoes reactions that allow it to regain the 18-electron configuration, while the corresponding ferrocenium ion does not.[18]

This difference can also be gathered upon direct addition of ferrocene as internal reference to the CH_2Cl_2 solution of **2**. Whereas the oxidation of ferrocene occurs at 0.54 V (290.8 nA), **2** does not show a clear oxidation peak anymore; instead, decomposition takes place immediately (Supporting Information, Figure S9). Obviously, ferrocene even enhances the irreversible reduction of $\mathbf{2}^+$. In summary, our experiment shows that **2** exhibits a much lower solubility and both a lower chemical as well as electrochemical stability than the homologous ferrocenyl-decorated Sn/S complex. It should be mentioned, however, that there exist ruthenocene-related complexes that do not differ so much from their iron analogues, such as those reported recently for $[Cp'Fe(\mu\text{-}C_{10}H_8)MCp^*]$ (M = Fe vs Ru), which showed only minor differences in the electronic structures.[19]

To further characterize the compound, we performed time-resolved photoluminescence (TRPL) measurements on single crystals of **2**. A series of measurements was carried out to characterize the optical response and investigate any changes to the emission characteristics, for instance, by optically induced structural, morphological, or chemical changes. Therefore, we illuminated a single crystal using the frequency-double emission from a pulsed 100 fs Ti:sapphire laser at 375 nm (3.3 eV) for 120 s. The individual measurements were repeated every 30 min, carefully avoiding any irradiation of the sample between two measurements. A standard streak camera setup was used for detection.[20] The whole setup provides a spectral resolution of 1 nm and a time resolution of 1 ps. Additionally, the sample was imaged on a high-resolution charge-coupled device video camera instead of the entrance slit of the spectrometer for optical control. This system provides a spatial resolution better than 5 μm, ensuring that we address individual single crystals with the 20 μm diameter laser focus. The crystals were kept in a controlled nitrogen-gas environment directly after taking them out of growth solution to avoid oxidation or other chemical reactions during the measurements. To exclude photoinduced changes of the crystal, we used a low excitation density of about 1 W/cm^2.

The PL spectra are shown in Figure 4 (left). The emission exhibits a broad peak; its maximum is centered at 500 nm (2.45

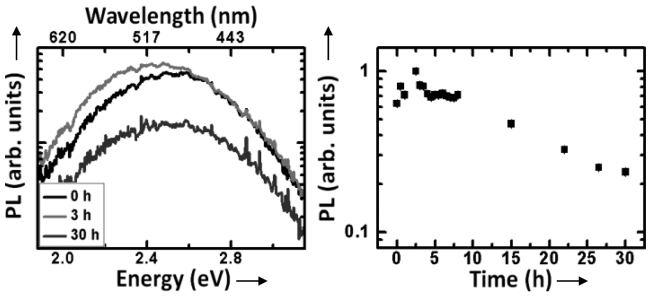

Figure 4. (left) Selected luminescence spectra of the long-term measurement of a single crystal of **2**. (right) Integrated luminescence intensity of all spectra, normalized to that of highest intensity.

eV). During long-term investigations, the following changes were observed: the lower-energy emission tail was enhanced during the first 3h. This was followed by quenching of the whole spectrum. To summarize these observations the integrated luminescence intensities are plotted as a function of time in Figure 4 (right). The enhancement of the lower-energy emission results in an overall increase by a factor of 2. Then, the intensity remains constant for a few hours, forming a small plateau before it eventually decreases by nearly an order of magnitude during the following day of irradiation.

dx.doi.org/10.1021/ic500367y | Inorg. Chem. 2014, 53, 4228−4233

The transients corresponding to the spectra shown in Figure 4 (left) are given in Figure 5 (left). They clearly exhibit a

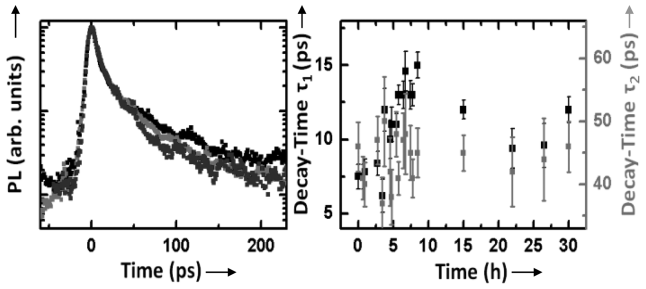

Figure 5. (left) Transients of selected spectra of a single crystal of compound **2**. (right) Fast (τ_1) and slow (τ_2) decay times of a double-exponential fit to the transients.

double-exponential decay. The resulting time constants are plotted in the right-hand panel of Figure 5. This indicates that dark states are involved in the decay processes.[21] The faster decay time (τ_1) is thus attributed to the actual radiative recombination. The second, slower component (τ_2) is due to population and depopulation of dark states. To further investigate the changes in the decay times the values obtained by a double-exponential fit of the data are shown in Figure 5 (right). The progression of the (τ_1) is very similar to that of the integrated intensity while (τ_2) stays rather constant. Both the enhancement in intensity on the low energy tail and the increase in decay time indicate the formation of additional defect-induced recombination channels in the crystal. This is attributed to evaporation of solvent from the growth solution trapped inside the crystal. This changes the crystal morphology, probably changes the structure on the atomic level, and leads to the formation of additional recombination channels. The decrease of the emission intensity at later times, however, is attributed to chemical degradation of the surface after the solvent is removed. This is corroborated by the overall quenching of the fast decay time (τ_1). A possible reactant for this degradation process is the evaporated solvent.

To investigate and exclude photoinduced damage effects as the origin of the changes, we performed one measurement with an excitation density of 30 W/cm^2 after the long-term study. The resulting spectra, as well as the corresponding transients, are shown in Figure 6. Most notably, the τ_1 decay time is significantly reduced, while the τ_2 time remains unaffected. In addition, the spectrum shows a slight decrease of the low-energy flank. The change in spectral shape indicates that the

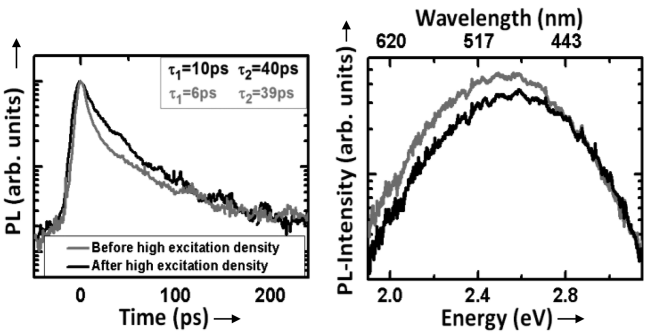

Figure 6. Transients (left) and spectra (right) of a single crystal of **2**, before and after illumination with high excitation density.

crystal is annealed by the radiation, as the defect-induced channels vanish at least partially. Increasing the τ_1 time, however, is presumably due to cleaning the crystal surface by the high radiation intensity.

For comparison, we performed similar long-term measurements on the known ferrocenyl-decorated analogue $[(R^{Fc}Sn)_4Sn_2S_{10}]$ (R^{Fc} = $CMe_2CH_2C(Me)$=N−N=C(Me)-Fc)[13] mentioned in the introduction. The luminescence spectra (shown in Figure 7) resemble those of the ruthenocene

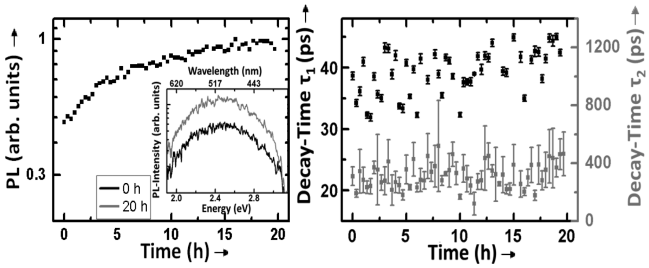

Figure 7. (left) Spectrally integrated PL intensity before and after long-term measurement of the ferrocenyl-decorated Sn/S cluster $[(R^{Fc}Sn)_4Sn_2S_{10}]$ (R^{Fc} = FcC(Me)CMe_2CH_2C(Me)=N−N=C-(Me)).[13] (inset) Exemplary spectra at early and later times. (right) Corresponding fast (τ_1) and slow (τ_2) decay times of the double exponential fits.

clusters. In case of the integrated intensity, however, the long-term time evolution shows a clear difference compared to that of the ruthenocene cluster **2** (c.f. Figure 4). While the latter exhibit a steep rise in intensity followed by a slow drop, the ferrocenyl-decorated species show a slow rise in intensity that levels out. As with compound **2**, this rise in intensity at early exposure time is attributed to laser-induced evaporation of the solvent from the crystal. This is further emphasized by a slight increase in of the fast component of the decay time. The lack of further changes on the long time scale, combined with the observation of reversible cyclovoltammetry[13] underlines the much larger chemical stability of the ferrocenyl-decorated cluster. In agreement with the electrochemical measurements of the ruthenocenyl-decoreated cluster **2**, this clearly confirms that the long-term changes of the latter are due to chemical changes.

■ CONCLUSION

We presented the first ruthenocenyl-decorated chalcogenide cluster known to date, $[(R^{Rc}Sn)_4Sn_2S_{10}]$ (R^{Rc} = CMe_2CH_2C-(Me)=N−N=C(Me)Rc), and discussed the synthesis, crystal structure, electrochemical stability, and time-resolved PL properties of this congener in comparison with the recently reported ferrocenyl analogue. Our findings show that it is possible to address similar synthetic goals with Fe replaced by Ru atoms on the surface of cluster molecules, but that the resulting compound is much more sensitive to air, electrochemical treatment, and irradiation. The latter is manifested in a noncyclable oxidation behavior that is followed instantly by decomposition of the compound and by a successive degradation of the emission intensity due to light-induced trap states following a short-term photoannealing. The ruthenocenyl-decorated chalcogenide cluster is thus significantly more affected by laser irradiation than the ferrocenyl analogue.

dx.doi.org/10.1021/ic500367y | Inorg. Chem. 2014, 53, 4228−4233

■ ASSOCIATED CONTENT

Supporting Information

Further X-ray data of compound **1**, NMR data, mass spectra, EDX of **2**, and cyclovoltammogram of **2** in the presence of ferrocene. This material is available free of charge via the Internet at http://pubs.acs.org.

■ AUTHOR INFORMATION

Corresponding Author

*E-mail: dehnen@chemie.uni-marburg.de. Fax: (+49) 6421-282-5653.

Author Contributions

The manuscript was written through contributions of all authors. All authors have given approval to the final version of the manuscript.

Notes

The authors declare no competing financial interest.

■ ACKNOWLEDGMENTS

We thank Christian Prinzisky for his help with CV measurements, Dr. Johanna Heine for her help with the structure refinements, Zhiliang You for the synthesis of $[(R^{Fc}Sn)_4Sn_2S_{10}]$, and the DFG for financial support of our work within the framework of SFB 1083.

■ REFERENCES

(1) (a) Kealy, T. J.; Pauson, P. L. *Nature* **1951**, *168*, 1039−1040. (b) Miller, S. A.; Tebboth, J. A.; Tremaine, J. F. *J. Chem. Soc.* **1952**, 632−635.

(2) Wilkinson, G. *J. Am. Chem. Soc.* **1952**, *74*, 6146−6147.

(3) (a) Vol'kenau, N. A.; Bolesova, I. N.; Shul'pina, L. S.; Kitaigorodskii, A. N.; Kravtsov, D. N. *J. Organomet. Chem.* **1985**, *288*, 341−348. (b) Rausch, M. D.; Fischer, E. O.; Grubert, H. *J. Am. Chem. Soc.* **1960**, *82*, 76−82.

(4) Recent examples: (a) MacDonald, D. G.; Kübel, C.; Corrigan, J. F. *Inorg. Chem.* **2011**, *50*, 3252−3261. (b) MacDonald, D. G.; Eichhöfer, A.; Campana, C. F.; Corrigan, J. F. *Chem.—Eur. J.* **2011**, *17*, 5890−5902. (c) Sawamura, M.; Kuninobu, Y.; Toganoh, M.; Matsuo, Y.; Yamanaka, M.; Nakamura, E. *J. Am. Chem. Soc.* **2002**, *124*, 9354−9355. (d) González-Rodríguez, D.; Carbonell, E.; de Miguel Rojas, G.; Castellanos, C. A.; Guldi, D. M.; Torres, T. *J. Am. Chem. Soc.* **2010**, *132*, 16488−16500. (e) Chen, J.; Lalancette, R. A.; Jäkle, F. *Chem. Commun.* **2013**, *49*, 4893. (f) Neidlinger, A.; Ksenofontov, V.; Heinze, K. *Organometallics* **2013**, *32*, 5955−5965. (g) Braga, S. S.; Silva, A. M. S. *Organometallics* **2013**, *32*, 5626−5639. (h) Hildebrandt, A.; Lang, H. *Organometallics* **2013**, *32*, 5640−5653. (i) Musgrave, R. A.; Russell, A. D.; Manners, I. *Organometallics* **2013**, *32*, 5654−5667. (j) Schaarschmidt, D.; Lang, H. *Organometallics* **2013**, *32*, 5668−5704.

(5) Recent examples: (a) Petrov, A. R.; Jess, K.; Freytag, M.; Jones, P. G.; Tamm, M. *Organometallics* **2013**, *32*, 5946−5954. (b) Madalska, M.; Lönnecke, P.; Ivanovski, V.; Hey-Hawkins, E. *Organometallics* **2013**, *32*, 5852−5861. (c) Klapp, L. R. R.; Bruhn, C.; Leibold, M.; Siemeling, U. *Organometallics* **2013**, *32*, 5862−5872.

(6) (a) Tang, J.; Top, S.; Vessières, A.; Sellier, N.; Vaissermann, J.; Jaouen, G. *Appl. Organomet. Chem.* **1997**, *11*, 771−781. (b) Burrell, A. K.; Campbell, W. M.; Officer, D. L.; Scott, S. M.; Gordon, K. C.; McDonald, M. R. *J. Chem. Soc., Dalton Trans.* **1999**, 3349−2254. (c) Nakamura, E. *J. Organomet. Chem.* **2004**, *689*, 4630−4635. (d) Wang, H. J. H.; Jaquinod, L.; Olmstead, M. M.; Vicente, M. G. H.; Kadish, K. M.; Ou, Z.; Smith, K. M. *Inorg. Chem.* **2007**, *46*, 2898−2913. (e) Liu, C.-G.; Guan, X.-H.; Su, Z.-M. *Comput. Theor. Chem.* **2011**, *963*, 98−103. (f) Nakamura, E. *J. Organomet. Chem.* **2004**, *24*, 4630−4635. (g) Grocka, I.; Latos-Grażyński, L.; Stępień, M. *Angew. Chem., Int. Ed.* **2013**, *52*, 1044−1048; *Angew. Chem.* **2013**, *125*, 1078−1082.

(7) (a) Braunschweig, H.; Hupp, F.; Kramer, T.; Mager, J. *Inorg. Chem.* **2013**, *52*, 9060−9065. (b) Vogel, U.; Lough, A. J.; Manners, I. *Angew. Chem., Int. Ed.* **2004**, *43*, 3321−3325; *Angew. Chem.* **2004**, *116*, 3383−3387. (b) Schachner, J. A.; Tockner, S.; Lund, C. L.; Quail, J. W.; Rehahn, M.; Müller, J. *Organometallics* **2007**, *26*, 4658−4662. (c) Andrikopoulos, P. C.; Armstrong, D. R.; Clegg, W.; Gilfillan, C. J.; Hevia, E.; Kennedy, A. R.; Mulvey, R. E.; O'Hara, C. T.; Parkinson, J. A.; Tooke, D. C. *J. Am. Chem. Soc.* **2004**, *126*, 11612−11620. (d) Yoshida, T.; Shinohara, T.; Onitsuka, K.; Ozawa, F.; Sonogashira, K. *J. Organomet. Chem.* **1999**, *574*, 66−76. (e) Zheng, N.; Lu, H.; Bu, X.; Feng, P. *J. Am. Chem. Soc.* **2006**, *128*, 4528−4529.

(8) Krebs, B. *Angew. Chem., Int. Ed. Engl.* **1983**, *22*, 113−134.

(9) (a) Berwe, H.; Haas, A. *Ber. Bunsen-Ges.* **1987**, *120*, 1175−1182. (b) Dakternieks, D.; Jurkschat, K.; Wu, H.; Tiekink, E. R. T. *Organometallics* **1993**, *12*, 2788−2793. (c) Wraage, K.; Pape, T.; Herbst-Irmer, R.; Noltemeyer, M.; Schmidt, H.-G.; Roesky, H. W. *Eur. J. Inorg. Chem.* **1999**, 869−872. (d) Wagner, C.; Raschke, C.; Merzweiler, K. *Appl. Organomet. Chem.* **2004**, *18*, 147. (e) Davies, A. G.; Smith, L.; Smith, P. J. *J. Organomet. Chem.* **1972**, *39*, 279−288. (f) Dörfelt, C.; Janeck, A.; Kobelt, D.; Paulus, E. F.; Scherer, H. *J. Organomet. Chem.* **1968**, *14*, P22−P24.

(10) (a) Hassanzadeh Fard, Z.; Müller, C.; Harmening, T.; Pöttgen, R.; Dehnen, S. *Angew. Chem.* **2009**, *121*, 4507−4511; *Angew. Chem., Int. Ed.* **2009**, *48*, 4441−4444. (b) Hassanzadeh Fard, Z.; Xiong, L.; Müller, C.; Hołyńska, M.; Dehnen, S. *Chem.—Eur. J.* **2009**, *15*, 6595−6604. (c) Heimann, S.; Hołyńska, M.; Dehnen, S. *Chem. Commun.* **2011**, *47*, 1881−1883. (d) Varga, R. A.; Silvestru, C. *Acta Crystallogr.* **2007**, *E63*, m2798.

(11) (a) Hassanzadeh Fard, Z.; Halvagar, M. R.; Dehnen, S. *J. Am. Chem. Soc.* **2010**, *132*, 2848−2849. (b) Halvagar, M. R.; Hassanzadeh Fard, Z.; Dehnen, S. *Chem. Commun.* **2010**, *46*, 4716−4718. (c) Halvagar, M. R.; Hassanzadeh Fard, Z.; Dehnen, S. *Chem.—Eur. J.* **2011**, *17*, 4371−4374. (d) Barth, B. E. K.; Leusmann, E.; Harms, K.; Dehnen, S. *Chem. Commun.* **2013**, *49*, 6590−6592. (e) Eußner, J. P.; Barth, B. E. K.; Leusmann, E.; You, Z.; Rinn, N.; Dehnen, S. *Chem.—Eur. J.* **2013**, *19*, 13792−13802.

(12) Gielen, M. *Tin Chemistry: Fundamentals, Frontiers, and Applications;* Davies, A. G., Pannell, K., Tiekink, E., Eds.; John Wiley & Sons: Hoboken, NJ, 2008; pp. 290f.

(13) (a) You, Z.; Fenske, D.; Dehnen, S. *Dalton Trans.* **2013**, *42*, 8179−8182. (b) You, Z.; Dehnen, S. *Inorg. Chem.* **2013**, *52*, 12332−12334.

(14) (a) Herberhold, M.; Steffl, U.; Milius, W.; Wrackmeyer, B. *Angew. Chem.* **1996**, *108*, 1927−1928; *Angew. Chem., Int. Ed.* **1996**, *35*, 1803−1804. (b) Herberhold, M.; Steffl, U.; Milius, W.; Wrackmeyer, B. *Z. Anorg. Allg. Chem.* **1998**, *624*, 386−392. (c) Bera, H.; Braunschweig, H.; Oechsner, A.; Sigritz, R.; Seeler, F. *J. Organomet. Chem.* **2010**, *695*, 2609−2613. (d) Wendji, A. S.; Lutter, M.; Dietz, C.; Jouikov, V.; Jurkschat, K. *Organometallics* **2013**, *32*, 5720−5730. (e) Dietz, C.; Jouikov, V.; Jurkschat, K. *Organometallics* **2013**, *32*, 5906−5917. (f) Chen, J.; Lalancette, R. A.; Jäkle, F. *Organometallics* **2013**, *32*, 5843−5851.

(15) (a) Sheldrick, G. M. *Acta Crystallogr., Sect. A* **2008**, *64*, 112. (b) Sheldrick, G. M. *SHELXL-2013;* University of Göttingen: Germany, 2013.

(16) Dolomanov, O. V.; Bourhis, L. J.; Gildea, R. J.; Howard, J. A. K.; Puschmann, H. *J. Appl. Crystallogr.* **2009**, *42*, 339−341.

(17) Hardgrove, G. L.; Templeton, D. H. *Acta Crystallogr.* **1959**, *12*, 28−32 (CSD-CYCPRU).

(18) Swarts, J. C.; Nafady, A.; Roudebush, J. H.; Trupia, S.; Geiger, W. E. *Inorg. Chem.* **2009**, *48*, 2156−2165.

(19) Malberg, J.; Lupton, E.; Schnöckelborg, E.-M.; de Bruin, B.; Sutter, J.; Meyer, K.; Hartl, F.; Wolf, R. *Organometallics* **2013**, *32*, 6040−6052.

(20) Chernikov, A.; Horst, S.; Koch, M.; Volz, K.; Chatterjee, S.; Koch, S. W.; Wassner, T. A.; Laumer, B.; Eickhoff, M. *J. Lumin.* **2010**, *130*, 2256−2259.

(21) Jones, M.; Lo, S. S.; Scholes, G. D. *J. Phys. Chem. C* **2009**, *113*, 18632−18642.